Pre-computed Data-driven Free Fall Animation

Haoran XIE* and Kazunori Miyata†

Japan Advanced Institute of Science and Technology

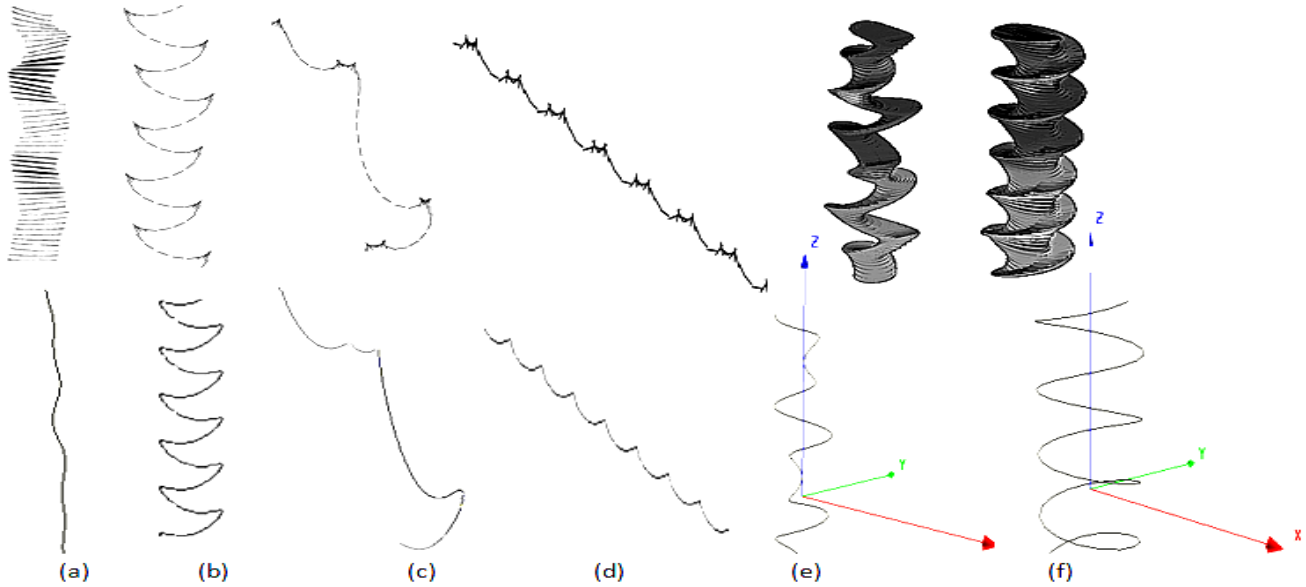

Figure 1: *Five measured trajectories (top, worked by [FIELD 1997; ANDERSEN 2005; ZHONG 2011]) and synthesized trajectories by our work (bottom) of the basic motion prototypes in free fall which are described in the phase diagram, (a) Steady Decent, (b) Periodic Fluttering, (c) Transitional Chaotic motion, (d) Periodic Tumbling, (e) Transitional Helix motion, (f) Periodic Spiral motion*

Abstract

Free fall motions, such as fluttering (oscillate from side to side) and tumbling (rotate and drift sideways) of lightweight objects or objects in the strong resistance fluid with high Reynolds number, are spectacular and familiar but we lack the predicable and realistic simulation of the phenomena in computer animation and other related fields. We propose a new data-driven approach for procedural motion synthesis by using free fall motion graphs in interactive environments. Six motion prototypes are defined in phase diagram and synthesized separately using trajectory search tree and pre- computed trajectory database. In motion graph, we decide the motion types of object in designated initial conditions and the motion types are constituted by motion prototypes. To get more natural and pleasing motion paths, we combine numerical simulation and experimental results of this topic from Physics. Depending on the data from thousands of experiments, we can simulate the unresolved physical problem, including chaotic motions or motions in three dimensional environments successfully by our approach. Other physical characteristics in free fall, such as rotation, are also figured out well. Optimizations are proposed for synthesized results by practical experiments to adjust and achieve a reasonable visual quality of the phenomena.

Keywords: physically-based animation, trajectory database, motion planning, free fall, motion prototypes, motion types

*e-mail: xiehr@jaist.ac.jp

†e-mail: miyata@jaist.ac.jp

1. Introduction

The realistic visual simulations of natural phenomena are important research field in computer graphics. Recently physically based simulation has been greatly developed, such as fluid simulation, rigid-body, and hair simulation. But we found that the common and spectacular free fall motion has been ignored and considered as an impossible work due to its intricately intertwined dynamics. In daily life, anyone must have noticed the falling motions of a paper or a leaf, sometimes it looks like regular, sometimes it is so random that we cannot find the rules hidden easily in the particular phenomena. Not all falling objects travel straight downwards which are normal in rigid-body simulation. This is due primarily to the coupling of forward motion to lateral oscillations by the surrounding fluid. The problem of free falling motions is rich in hydrodynamic effects, including lift, drag and vortex shedding, exhibiting both regular and apparently chaotic behavior. It is a challenging task and relevant to unsteady dynamics, meteorology, flight aerodynamics, sedimentology, bubble rising and boiling, seed dispersal, and all visual simulations about the aforementioned fields in computer graphics.

There are three traditional ways to obtain realistic motion animation: key frame control, physically-based simulation, motion capture. We consider that all of these approaches are not available in the following reasons: (1) Creating motions by key frame requires numerous efforts and expert ability for animators; (2) Even the physically-based simulation can make a reliable result but it only fit for simple models. Until now, there is no numerical simulation which can resolve chaotic motion and free motion in three dimensional successfully. (3) Motion

capture is not only expensive to use due to time consuming and difficult to capture the exactly data which we want for the complex dynamic in free fall motions and dependence of specific circulation, but also is not possible to capture motion data using 3D marker and difficult to control the cameras, especially in chaotic case.

In this work, we present new approaches combining both experimental and theoretical results about the topic in physics, and completely examine all the motion types in free fall motion of light-weight objects to create reliable and natural motion paths by using motion planning in real time environment. The following are our key contributions:

Trajectory Search Tree: We have compared the trajectories of periodic fluttering, tumbling and chaotic motion trajectories from actually measured data, and found that there is a choice problem when the object arrives to the turning points, in the mean time, chaotic motion happened if objects oriented vertically at turning points (see Figure 1 (c)). In this condition, we can mix the motion segments of fluttering, considering that the chaotic trajectories is an unstable and transitional region between fluttering and tumbling motion.

Pre-computed Trajectory Database: Since the motion of free fall is complex, it needs a plenty of memory cost consuming if using numerical simulations, which is not appropriate for real time applications. Our approach is to calculate the position and orientation off-line and stored as a database of motion segments. This database then is used by choosing proper feature vectors from on-line environments. Our database included about 1200 motion segments including the data of positions and calculated orientations. The orientation is depending on the interpolation of data by solving ordinary differential equations. We generate motion by piecing together example motions from the database.

Free Fall Motion Graph: We have developed a specific motion graph based on six motion prototypes (Figure 1) in phase diagram of free fall. We can construct the whole motion path by selecting sequence of nodes from different motion prototypes. By analyzing the motion data of thousands of experiments in experimental physic, we make a discovery about the motion selection which never be presented neither physics nor computer graphic researches: There are 35 kinds of potential motion types for free fall motion in the case of period spiral phase for example. Also the probability of motion selection is created to get numerous realistic but differential motion paths.

The remainder of this paper is organized as follows. Related work is described in Section 2. In Section 3, we present an overview of our system to solve the problem in the motion synthesis, and final trajectory construction. The relation between initial condition and phase diagram are introduced in Section 4. Section 5 describes the motion synthesis of six distinct motion prototypes in free fall motion by using trajectory search tree and pre-computed trajectory database. In Section 6, we design a specific free fall motion graph for path construction based on motion prototypes, motion constraints are discussed which are found in thousands of experiment data. The simulation optimizations and results are demonstrated in Section 7 and Section 8. Finally, we draw conclusions and discuss the limitation and future work.

2. Related Work

Free fall simulation has a rich history in fluid mechanics but few realistic simulations have been done in computer graphics.

Scientific interest in the phenomenon dates back to one and half century ago, Maxwell noticed the torque by the gravity and lift [MAXWELL 1854]. Until most recently, the phase diagram for falling disks with fluttering, tumbling, and steady decent was measured [WILLMARTH 1965]. In Tanabe and Berlmonte papers [TANABE 1994; BELMONTE 1998], five different falling patterns were discovered and the transition from fluttering to tumbling occurs at special Froude number by solving ordinary differential equations based on Kutta-Joukowsky theorem. The chaotic motion was also described and tumbling, and more detailed phase diagram was presented according to I^* and Re [FIELD 1997]. The direct numerical simulations of two-dimensional Navier-Stokes equation and a fluid force model were also derived from experiments [ANDERSEN 2005]. However, all these models are built in two dimensional space or quasi-two-dimensional setup. Most recently, a complete investigation [RAZAVI 2010] concerned about the relationship between different parameters which can affect different paths of motion in leaves based on more than six thousands experiments. Another experimental research found other three typical trajectories in three-dimensional environment: zigzag, transitional and spiral [ZHONG 2011]. There are still no convincing numerical simulation can explain the chaotic motion and free fall in three dimensional spaces.

The research of complete free fall simulation is not so satisfying in computer graphics. In the scarce physically-based simulations, Wei et al. [WEI 2003] used LBM method for wind simulation and rendered soap bubbles and a feather as results, but we cannot obtain the required motion paths which are normal in daily life for animator, also it is very heavy for simulating multiple objects due to the particle method consuming computational cost. Other related example-based approaches were based on Markov model [REISSELL 2001], captured videos [AOKI 2004], segments from fluid Simulation [SHI 2005], Maya production [VAZUQUEZ 2008], sketch example [LI 2010]. All these simulations ignored the nature of free fall and considered the free fall motion as a complete complex and unpredictable dynamics using stochastic processes or simple particles presentation. Some commercial CG tools, including Lightwave, Maya, etc. are actually loss of free fall animation, also using particle simulation for falling objects by control the drag and lift parameter in wind field [KELLER 2010]. In these cases, the motion paths are unpredictable and not easy to be controlled and modified for the required motions.

Motion synthesis, data-driven motion editing and synthesis typically address human motion. In early years, data warping and sign processing were adopted. Recent works on data-driven motion synthesis build on a graph with transitions between nodes where a smooth motion is possible [KOVAR 2002; ARIKAN 2002]. Other interesting related works are these concerning the oscillations in the motion synthesis and unsteady dynamics, including rain streaks [GARG 2006], bubble rising [HONG 2003], kite flying [OKAMOTO 2009].

3. System Overview

A data diagram of our system is shown in Figure 2. The inputs of our system are the initial conditions and input parameters of a lightweight object with 6 degree of freedoms (DOFs), including the physical characteristics of the object and fluid wherein released (release height, mass, etc.). We transform the parameters to the two important non-dimensional numbers Re and I^*, and lookup the phase diagram of free fall to query the motion level in which the object motion is stable.

After the motion level of motion prototypes is decided, we first decide the motion types category based on the level. In all kinds of the motion types of the decided motion category, probability model is adopted to choose the actual motion paths. In our work, the motion trajectory is constructed from six motion sequences of motion prototypes. The free fall motion graphs are the used to synthesis the trajectories from the

designated motion segments. After optimization to the initial trajectories, Final free fall paths are synthesized (Figure 1).

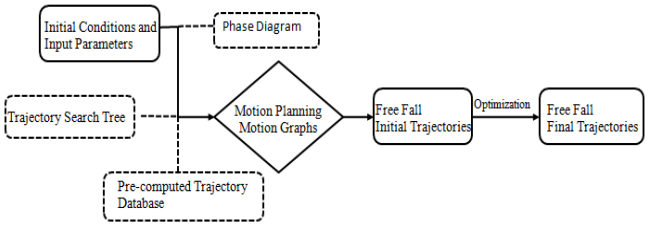

Figure 2: System overview

4. Free Fall Phase Diagram

A falling object is characterized by the following parameters: The height to release, h; the length of object, l; the length and width of the cross section, a and b (Namely, a is the width and b is thickness of the object; In the case of ellipse, l and a are the major and minor axes; If circular, l=a is diameter); the density of the object, ρ_s; and the density of the fluid, ρ_f; the kinematic viscosity of the fluid, v; and the gravity acceleration, g. From these parameters, three dimensionless quantities: the Reynolds number, Re; the aspect ratio of object, e=b/a; the dimensionless moment of inertia, *I** (See Appendix)

$$\mathrm{Re} = \frac{\mathrm{Ua}}{\mathrm{v}} \quad (1)$$

In (1), U is average descent velocity of the object, the simple estimate of U is

$$\mathrm{U} \sim \sqrt{\mathrm{gb}\left(\frac{\rho_s}{\rho_f} - 1\right)} \quad (2)$$

For the lightweight objects, b is very small, so e (e<<1) is so small that has no effect on the motion of free fall objects.

Based on the work by [WILLMARTH 1964; STRINGHAM 1969; FIELD 1997; ZHONG 2011], the phase diagram is shown in Figure 3, which can decide the main motion of free fall object by *Re* and *I**. Note that, we cannot decide the whole motion paths simply only depend on the phase diagram, as we explained in related work, the experimental setups of these work are totally two dimensional.

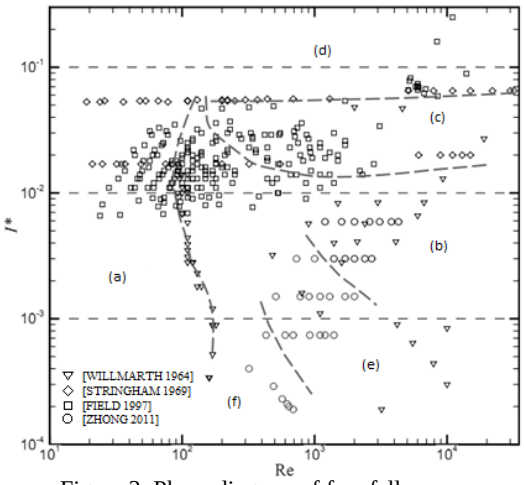

Figure 3: Phase diagram of free fall

In Figure 3, the free fall motion can be divided into six motion prototypes (Figure 1) which belong to two kinds of motion: steady and unsteady motion.

Steady motion:

(a) **Steady Decent (SD)**: the object drops down in vertical with horizontal orientation

Unsteady motions:

(b) **Periodic Fluttering (PF)**: the object oscillates from side to side with a well defined period

(c) **Transitional Chaotic motion (TC)**: the object tumbles and flutters, the number and time of tumbling and fluttering appears to be random

(d) **Periodic Tumbling (PT)**: the object turns continuously end-over-end and drifts in one direction

(e) **Transitional Helix motion (TH)**, the object moves in a helical path at constant speed

(f) **Periodic Spiral motion (PS)**: the object moves in a spiral path

5. Trajectory Synthesis of Motion Prototypes

In this section we give the details how to synthesis each motion prototypes, which can be incorporated to make the initial trajectories in the designated conditions.

5.1 Trajectories of TH and PS

When projecting the motion paths into XY plane which measured by [ZHONG 2011], we notice that the curves of six

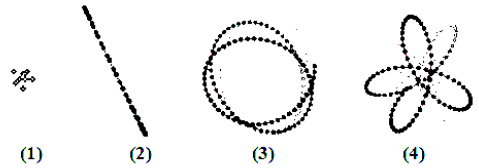

Figure 4: Measured paths projected into XY plane, (1) SD, (2) PF&PT&TC, (3) PS (4) TH

basic motion prototypes have characteristic shapes: SD is likely to be a point, PF, PT and TC are in one straight line, PS is similar to circle and TH is similar to 8 petals rose curve. In the XY plane, trajectories consist of two parts of motion: (1) Rotation about the vertical fall direction, (2) A harmonic elliptical oscillation which oscillate in both x and y direction meanwhile. The curves are expressed as following equation:

$$x(t) = A\cos(\Omega t)\,(1 + B\sin(k\Omega t)) \quad (3)$$

$$y(t) = A\sin(\Omega t)\,(1 + B\sin(k\Omega t)) \quad (4)$$

$$z(t) = h - Ut \quad (5)$$

where A is the amplitude of the elliptical oscillation happened in XY plane orientation, B is ratio of the short axis and long axis of the ellipse, k is the ratio of the period of the elliptical oscillation to the period of rotation. Ω is the angular frequency of the motion, U is the descent velocity in Equation (2). So

1. B→0 k=1: PS
2. A→0 k=0: SD
3. B≠0 k=4: TH

The synthesized trajectories are presented as (a), (e) and (f) in the bottom of Figure 1.

About PF, PT and TC motion prototypes, we explain as follows.

5.2 Trajectories of PF, PT and TC

In this subsection, the motion trajectories of fluttering, tumbling and chaotic motion are synthesized by a tree structure which conforms to the experimental measured data. Then, motion segments are obtained from harmonic functions and interpolated orientations from solving ordinary differential equations (ODEs) of force model of free fall. We store the motion segments into a pre-computed trajectory database after clustering variety of motion segments. At the end, the result of synthesized trajectories is presented.

5.2.1 Trajectory Search Tree

We compare the trajectories of chaotic motion, periodic

fluttering and tumbling motion in experiments. Beside the airflow behind the free fall object reveals vortex shedding, turbulence and other complex motion, the object comes to

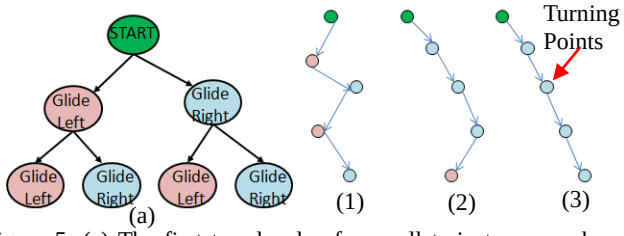

Figure 5: (a) The first two levels of a small trajectory search tree; In (1), (2) and (3), PF, TC and PT are created by traversal four levels of search tree. The three tree structures are correspond to (b), (c) and (d) in Figure 1.

turning points, where the angular velocity becomes 0 and the velocity in the oscillation direction also be 0 but in vertical direction be maximum value. The object face to two alternatives of sliding left or sliding right (flutter or tumble) due to the motion prototype it belong to in PF, PT and TC.

In Figure 5, we create a trajectory search tree, where start point is set as root and turning points as nodes. The edge between nodes is the motion segments from motion sequences. Note that the chaotic motion is defined by using different kinds of nodes, in other words, chaotic motion is the transition region between periodic fluttering and periodic tumbling. It is noticed that chaotic motion happened when the angle at turning points comes to orient vertically, the dynamic is much more sensitive to experimental noise than in the periodic regions (PF & PT).

5.2.2 Segmentation and Clustering

Segmentation: There are three ways to get motion segments which are used to present the transition between nodes of trajectory search trees:

(1) Particle methods

To solve Navier-Stokes equations, particle methods of Semi-Lagrange (STAM 1999) and Smoothed Particle Hydrodynamics (SPH) (FEDKIW 2001) are good alternatives. The trajectory of a particle start from tracing particle from frame to frame by following velocity vectors until last frame or the boundary has been reached. Many trajectories are obtained by empirically deciding the duration and number of fluid simulations.

Although it is a common way to use this way in most recent works as interpreted in Section 2, we do not adopt this approach, because 1). It cannot catch the nature of free fall motion, not be able to detect all the motion prototypes in our phase diagram. 2). The angular rate cannot be achieved correctly. 3). Required motion trajectories are difficult to be satisfied.

(2) Force model of free fall

When object falls freely, there are three forces play roles in the motion: lift, friction, gravity ([TANABE 1994]). The friction has two parts: perpendicular and parallel to the object. By the Kutta-Joukowski theorem, following ODEs are deduced.

$$\frac{du}{dt} = -(A_\perp \sin^2\theta + A_\parallel \cos^2\theta)u + (A_\perp - A_\parallel)\sin\theta\cos\theta v - k\pi\rho V^2\cos\beta\cos\alpha \quad (6)$$

$$\frac{dv}{dt} = -(A_\perp \cos^2\theta + A_\parallel \sin^2\theta)v + (A_\perp - A_\parallel)\sin\theta\cos\theta u + k\pi\rho V^2\cos\beta\sin\alpha - g \quad (7)$$

$$\frac{d\omega}{dt} = -A_\perp\omega - \frac{3\pi\rho V^2}{a}\cos\beta\sin\beta \quad (8)$$

$$u = \frac{dx}{dt} \quad (9)$$

$$v = \frac{dy}{dt} \quad (10)$$

$$\omega = \frac{d\theta}{dt} \quad (11)$$

$$\rho = \frac{\rho_f a}{\rho_s V_s},\ \beta = \alpha + \theta,\ V = \sqrt{u^2 + v^2} \quad (12)$$

In these equations, $A_\perp$,$A_\parallel$ are friction coefficients in perpendicular and parallel direction to the object. V_s is the volume of the object which is calculated by initial parameters. θ is the angle of paper, α=arctan(u/v) the angle of velocity (Figure 6 (a)). k is a sign coefficient,

if v*sin(β) >= 0 k=1

if v*sin(β) < 0 k=-1

In order to get the turning points position, additional constraints are necessary.

$$u = 0, \omega = 0 \quad (13)$$

We employ standard fourth-order Runge-Kutta method to solve the second-order ordinary differential equations. The result of fluttering case is shown in Figure 6 (b).

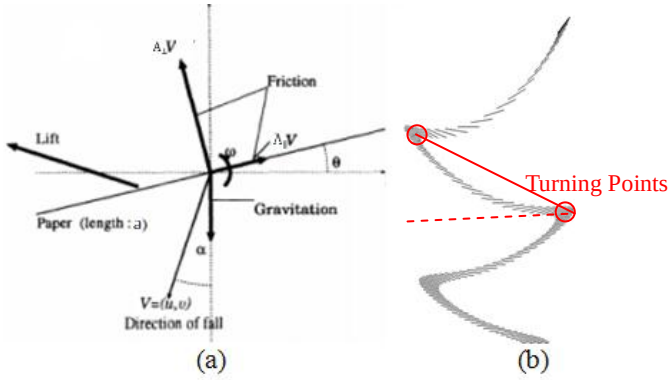

Figure 6: (a) Force model of free fall object; (b) The trajectory by solving ODEs $A_\perp$=4.1 $A_\parallel$=0.9

(3) Harmonic functions

Because the symmetry of the fluttering motion, the frequency of the oscillatory component of vertical velocity is twice of the horizontal velocity component. According to the measured data of experiments, we use harmonic functions to describe the generally complex planar motions.

$$x(t) = \frac{A_x}{\Omega}\sin(\Omega t) \quad (14)$$

$$z(t) = h - Ut - \frac{A_y}{2\Omega}\cos(2\Omega t) \quad (15)$$

where A_x and A_y are the amplitudes of vertical and horizontal velocities caused by the oscillation. Ω describes the angular frequency of the motion, the same as the parameter in Equation (3) (4).

Comparing the (2) and (3) segmentation both of which segmented by turning points, we find that harmonic is easily be controlled by gradually modification of parameters, so that the required trajectory segments are queried possibly and quickly what is quite different in the ODEs case due to the hard control of the curvatures of trajectories. We combine (2) and (3) approach so that we obtain the positions from (2) and orientations from (2).

Clustering: After the step of segmentation, there are numerous of segments obtained by tuning parameters in (14)&(15) in a designated step. We use K-means clustering algorithm [REISSELL 2001] for clustering data.

The input segments $\{S_i | i = 1, \ldots, N\}$ are classified based on the value of feature vectors of each segment by start and end

points. Feature vectors V $\{V_i | V_i = P_i^1 - P_i^0, i = 1, \dots, N\}$ (Figure 8) are assigned into K classes using K-means algorithm.

5.2.3 Pre-computed Trajectory Database

After clustering, we store the position R_i^k and orientation q_i^k $\{(R_i^k, q_i^k) | i = 1, \dots, M\}$ (M is the number of frames of the segmentS_k) of segment S_k into trajectory database.
About the orientation, we use the results of segmentation (2) for interpolation.
$\{(R_i^l, q_i^l) | i = 1, \dots, Q\}$ is the segment $S_l$of segmentation (2) with Q frames and feature Vector V*. We calculate the feature Vector V_k of segment S_k.
If the angle of $V_{k<=}$ V*, we find point j (1<<j<Q), let
$V_j \leq V_k < V_{j+1}$
We interpolate q^k with $\{q_i^l | i = 1, \dots, j\}$ by comparing positions $\{R_i^k | i = 1, \dots, M\}$ and $\{R_i^l | i = 1, \dots, j\}$ using linear interpolation.
If the angle of $V_{k>}$V*, we divide segment S_k into small parts and let the angle feature vector of every parts is not larger than V*, then use the same process of linear interpolation.

5.2.4 Motion Synthesis of PF, PT and TC

The fluttering and tumbling are periodic motion, so that we use the same segments but in different sliding orientation in the search tree (Figure 8).
Because the chaotic nature of TC motion, we synthesize the motion randomly with feature vector $V = rV_0$ and amplitude of oscillation $A = rA_0$. r is random number between 0.1 and 10 calculated by Box-Muller method, the angle of V_0 is initial feature vector defined as the release angle of the object, and A_0 is initial amplitude given in next section.

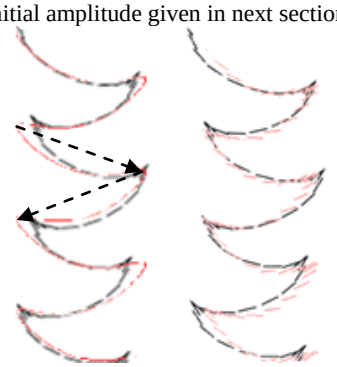

Figure 8: Comparison synthesized trajectory (Red) with measured data (Black) of fluttering motion, and the result of no orientation (left) and interpolated orientation (right). The arrow lines are feature vectors.

6. Free Fall Motion Graph

In this section, according to the 6000 experiments data in [RAZAVI 2010], we propose the rule how to connect motion prototypes and the motion selection based on probability model. Then we simulate the whole motion paths using free fall motion graph.

6.1 Connecting Motion Prototypes

In Figure 9, 7 motion groups are recorded which are illustrated in different colors. The arrow of the lines means the motion transition between different motion prototypes. If the arrow pointed itself, it means the motion happened independently. For example, the green line means that the object first tumble and then flutter in order; the black line means that only steady descent happened.

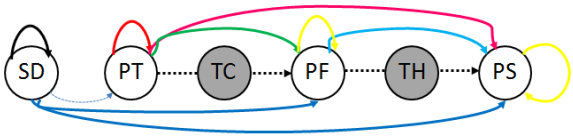

Figure 9: Motion groups in the experiments

In these experiments, *Re* is about 10^2, and *I** is 10^{-3}, so the main motion is PS. We notice that the motion transition is in the order SD→PT→PF→PS. Because TC is the transition region between tumbling and fluttering, and TH is also the transition region, Although TC and TH are not be considered in the experiment, we recognize the transition region have the similar characteristic with neighbor motion prototypes. So the number N of all kinds of motion types is revealed by:

$$N = \sum_{i=1}^{l} C_l^i \quad l \in [1,6] \tag{16}$$

where l is the level of motion types in the order SD→PS, For example, in the case of PS l=6, N becomes 35.

6.2 Probability Model

We can get the main motion of free fall object from the phase diagram according to the initial parameters, and the potential motion types are decided by the motion prototypes. Then we use probability model to decide which kind of specific motion paths of free fall. From the experiments we can get:

(1) Motion groups are distributed in normal distribution of Gaussian functions (Figure 10 (top))
$$f(r) = Ae^{-(\frac{r-B}{c})^2} \tag{17}$$
r is the spatial deviation from released point
(2) If the motion paths include tumbling, the deviation is linear relationship with the release height
$$B(h) = ah + b \tag{18}$$
h is the height, and it is possible that b=0,a~1 and in other cases, the deviation does not related to h.
(3) The deviation is independent of the size of shape in the same shape, so width-length ratio w/l is important

According to the three items, we get the spatial deviation of different motion prototypes.(Figure 10 (bottom)). And the deviation of PF, TC, TH, PS is
$D \sim \epsilon D_0 l/w$
where D_0 is the average deviation from Figure 10 (bottom), ϵ is the deviation coefficient. Because fluttering, spiral is periodic motion with constant amplitudeA_0=D (See Figure 4). About tumbling motions, the frequency of tumbling motion is$\Omega \sim b^{1/2} a^{-1}$ [MAHADEYAN 1999]. So we can obtain the initial amplitude of tumbling motion (PT).

$$A_0 = B(h)U/(h\Omega) \tag{19}$$

Through the statistical data from the experiments, we can get the probability of each motion prototypes.

$$P\left(\bigcup_{j=1}^{l} E_j\right) = \sum_{j=1}^{l} P(E_j) = 1 \tag{20}$$

E is one event in SD, PT, TC, PF, TH, PS, and l is the motion level obtained from the phase diagram. We get the probabilities from experimental data (0.1, 0.38, 0.1, 0.17, 0.11, 0.14 in the order of Figure 9), so that we decide the specific motions in designated motion types by probabilities.

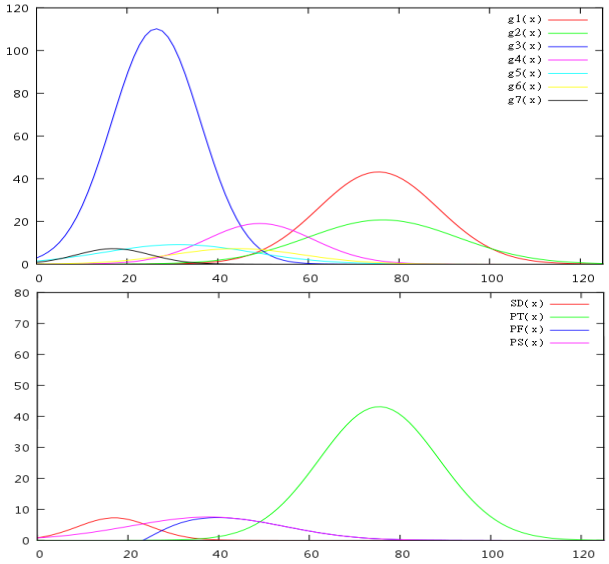

Figure 10: Spatial distribution of 7 motion groups (top) and motion prototypes (bottom), horizontal axis is the deviation from released position (cm); vertical axis is the quantity of the object, the released height is 125cm

6.3 Motion Graph

Six types of motion sequences are obtained by synthesis approach using initial parameters in Section 5 and calculated oscillation amplitudes (aforementioned). Every frame in these motion sequences can be a node; the edge between nodes is a transition splice in sequences.

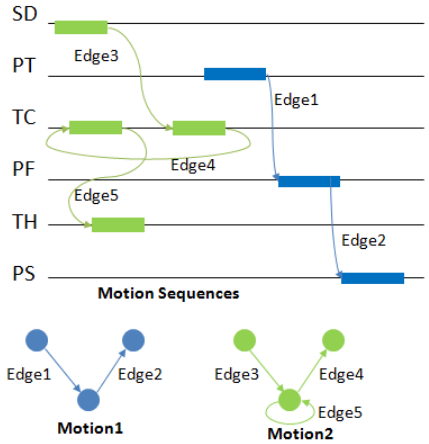

Figure 11: Free fall motion graph, a motion path represents a collection of splices between sequences (top) two example motions are represented by the directed graph.

We search the graph by probability function (6.2) in one-way from top to down, and synthesize a specific motion trajectory of free fall object.

7. Optimization

7.1 Smoothen curves

When we connect two motion sequences in different motion prototypes, C0 continuity is kept easily but C1 continuity is necessary in this case. We smoothen the motion rotations by using spherical linear interpolation and positions by linear interpolation. We choose the smoothing domain to be $\pm$n frames around connection points, defined as

$$\{(R_i^A, q_i^A)|i = Q - n + 1, \dots, Q\}\{(R_j^B, q_j^B)|j = 1, \dots, n\};$$

The k ($0 \le k < n$) frame in transition frames as follows:

$$R_k = \alpha(k)R^A_{Q+k-n+1} + (1 - \alpha(k))R^B_{1+k} \quad (21)$$

$$q_k = slerp\left(q^A_{Q+k-n+1}, q^B_{k+1}, \alpha(k)\right) \quad (22)$$

Where *slerp* is the spherical linear interpolation function. To keep the C1 continuity, conditions $\alpha(0) = 1\ \alpha(n) = 0, \frac{d\alpha}{dt}(0) = \frac{d\alpha}{dt}(n) = 0$ are necessary. The unique cubic polynomial satisfying these conditions is:

$$\alpha(t) = 2t^3 - 3t^2 + 1\ t = \frac{p}{n} \quad (23)$$

7.2 Rotation

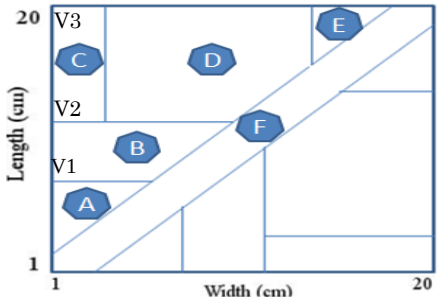

Figure 12: The relation between rotation and width-length ratio. A: fall perpendicular; B: Flutter in width axis→Rotation in width axis→rotation in length axis; C: Flutter in width axis; D:Flutter in width axis→rotation in length axis E: irregular F: Flutter in diagonal→rotation in diagonal

Figure 12 is summarized from experiment. We know the follows in three dimensional environments.

(1) When both length and width is small, SD happens
(2) Most motion starts form fluttering in width
(3) Rotation in length axis is the most stable motion, if the length is the same with the width axis, rotation in diagonal is most stable.

All these optimizations are included in our system. Note that the thresholds in the figure are defined as: V1=V2/2 which means bigger than this value objects start oscillation. V2 is Froude Number defined in [BELMONTE 1998], Fr=0.67= $(\frac{M}{\rho_s l^2 a})^{1/2}$ where M is mass of the object. V3 is the value in the phase diagram where chaotic motion occurs.

8. Results

Object	Fluid	Size	Result
Circle	Water	a=2.0cm b=0.15cm	Figure 13
Quasi-ellipse(Leaf)	Air	l=7.3cm a=4.2cm b=0.03cm	Figure 14
Ellipse	Air	l=8.0cm a=2.0cm b=0.01cm	Figure 15

Table 1: Experiment setups

While the example shown in Figure 13 suggests that our result is realistic, it is variable for not only air but all fluids where the object free fall. As shown in the left image, an aluminum circular disk had fallen in the water from 50 cm height. A looks regular fluttering motions are observed. According the initial parameter in Table 1, $I^*=10^{-2}$, and $Re=3.55*10^3$. By looking up the phase diagram, the main motion prototype is fluttering (PF). Then using our free fall motion graph and probability model, we get the positions and orientations from motion sequences constituted by pre-computed database, and the result is shown in right image.

Figure 14 shows a leaf falls in air from 200cm height, the perpendicular falling, tumbling and helix motions are found here. We calculated $I^*=6.3*10^{-3}$ and $Re=1.2*10^4$, so the main motion is transitional helix motion. The connection of three motion prototypes observed is well fit in out model. Between the connections among each motion sequences, the smoothen curve is presented in right image.

Finally, Figure 15 shows a red paper fallen in air, and $I^*=2.2*10^{-3}$ and $Re=6.8*10^3$, which is approximately spiral motion in the phase diagram. And the real motion is tumbling and spiral motion, which has verified our model right. According to the rotation in optimization, it fits type B and the simulation is flutter in length and rotation in length axes.

All examples were implemented on CPU. Because most parts of our approach are executed offline, the online motion synthesis and optimization process are rarely memory consuming, so our simulation is realistic and predictable, so is fit for interactive applications.

Figure 13: Comparison of our simulation with the real free fall of one Japanese yen coin in water

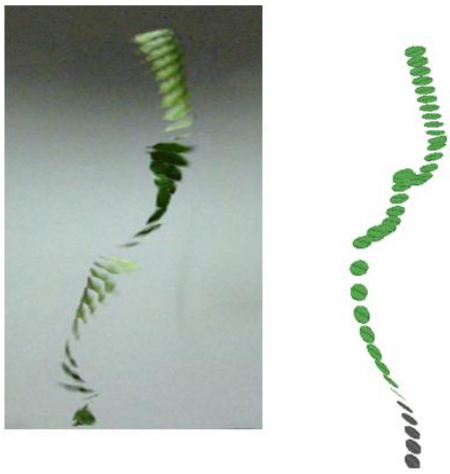

Figure 14: Comparison of our simulation with the real free fall of a leaf released from 2.0m height

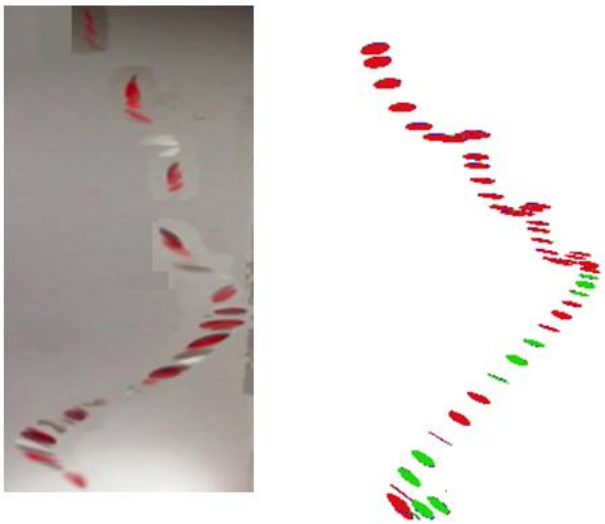

Figure 15: Comparison of our simulation with the real free fall of a red ellipse paper in air released from 3.1m height

9. Conclusion and Future-work

In this paper we have presented a framework for generating free fall animation by data-driven motion synthesis and pre-computed trajectory database. Our approach proposed six motion prototypes, maximum 35 kinds of motion types, and finally synthesized motion trajectories. This work is the first research about the details of free fall motion and proposes a efficient approaches to achieve a realistic and predictable simulation.

Ours work is for regular geometries, including quasi rectangular, circular, and elliptical objects with constant densities. For irregular geometry and uneven density distribution objects, it is complicated to consider the influence to the motion by the geometry and density distribution modifications. When paper or plastic object free fall, the change of shape also happen during the motion, which we omitted in our system. Finally, the initial angle is considered as initial value which constraints feature vector in Section 5, but we found that the released initial angle has great influence in free fall. It is still unsolved in science, only qualitatively described in [FIELD 1997], and as a result the angular velocity modifications are much complicated than the result of present researches, which are processed empirically by experimental observations in our work.

We conclude with a brief discussion of future work. Our free fall model is in still fluid environment, we would like to employ our simulation in wind field. We would like to improve the probability model in our work by using Bayesian Network, which represents conditional dependency and the relationship of events, so that we could predict the free fall motion more correctly.

Appendix

The dimensionless moment of inertia *I** indicates the inertial resistance of object to rotate and is defined as

$$I^* = \frac{I}{\rho_f a^5} \tag{24}$$

Where I is the moment of inertia of object, can be calculated by

$$I = \int_v \rho(x,y,z) \begin{bmatrix} y^2+z^2 & -xy & -xz \\ -xy & z^2+x^2 & -yz \\ -xz & -yz & x^2+y^2 \end{bmatrix} dxdydz \tag{25}$$

$\rho(x,y,z)$ is the density function.

The common cases of basic shapes are calculated:
Disk:

$$I^* = \frac{\pi b \rho_s}{64 \rho_f a} \quad (26)$$

Plate with rectangular cross-section:

$$I^* = \frac{8 \rho_s b (a^2 + b^2)}{3 \pi \rho_f a^3} \quad (27)$$

Plate with elliptical cross-section:

$$I^* = \frac{\rho_s b (a^2 + b^2)}{2 \rho_f a^3} \quad (28)$$

References

ANDERSEN, A., PESAVENTO, U. & WANG, Z. J. 2005 Unsteady aerodynamics of fluttering and tumbling plates. J. Fluid Mech. 541, 65–90.

AOKI, K., HASEGAWA,O. AND NAGAHASHI,H. 2004. Behavior Learning and Animation Synthesis of Falling Flat Objects. Journal of Advanced Computational Intelligence and Intelligent Informatics, vol.8, no.2, 100-107.

ARIKAN, O., AND FORSYTHE, D. 2002. Interactive motion generation from examples. In Proceedings of ACM SIGGRAPH 2002, Annual Conference Series, ACM SIGGRAPH.

BELMONTE, A., EISENBERG, H., AND Moses, E. 1998. From flutter to tumble: Inertial drag and Froude similarity in falling paper. Physical Review Letter. 81,345.

FEDKIW, R., STAM, J., AND JENSEN, H. W. 2001. Visual simulation of smoke. In Proceedings of SIGGRAPH 2001, Computer Graphics Proceedings, Annual Conference Series, 15-22.

FIELD, S., KLAUS, M., MOORE, M AND NORI, F. 1997. Chaotic dynamics of falling disks. Nature, 388, 252.

GARG, K. AND NAYAR, S. 2006. Photorealistic rendering of rain streaks. International Conference on Computer Graphics and Interactive Techniques SIGGRAPH, 996–1002.

HONG J.M., and KIM, C.H. 2003. Animation of bubbles in liquid. Computer Graphics Forum 22, 3, 253–262.

KELLER, E. 2010. Mastering Autodesk Maya 2011. Sybex. Chapter14, Dynamic Effects,749-780.

KOVAR, L., GLEICHER, M. AND PIGHIN, F. 2002. Motion graphs, Proceedings of the 29th annual conference on Computer graphics and interactive techniques, July 23-26, 2002, San Antonio, Texas.

LI, H., SUN, Q., ZHANG, H. AND ZHANG Q. 2010, Example-based motion generation of falling leaf, International Conference on Computer Design and Applications (ICCDA), 2010, vol.5, no., pp.V5-217-V5-221, 25-27.

MAHADEYAN, L., RYU,W.S. AND SAMUEL, A.D.T 1999. Tumbling cards. Phys. Fluids 11, 1–3.

MAXWELL, J. C. 1854 On a particular case of the descent of a heavy body in a resisting medium.Camb. Dublin Math. J. 9, 145–148.

MIHALEF, V., UNLUSU, B., SUSSAN, M., AND METAXAS, D. 2006. Physics-based boiling simulation. In Proceedings of SCA2006, Eurographics Association, 317–324.

OKAMOTO, T., FUJISAWA, M, AND MIURA, K. 2009. Interactive Simulation of Flying Japanese Kites, Sandbox 2009: ACM SIGGRAPH Video Game Proceedings, 47-53.

RAZAVI, P. 2010. On the Motion of Falling Leaves. Popular Physics, arXiv:1007.1769.

REISSELL, L. M., AND PAI, D. K. 2001. Modeling Stochastic Dynamical Systems for Interactive Simulation. Computer Graphics Forum 20, 3, 339-348.

SHI, L., YU, Y., WOJTAN, C., AND CHENNEY, S. 2005. Controllable Motion Synthesis in a Gaseous Medium. The Visual Computer, 21: 7, 474-487.

STAM, J. 1999, Stable Fluids. Proc. of ACM SIGGRAPH, pages 121–128.ACM, 23-30.

TANABE, Y. AND KANEKO, K. 1994. Behavior of a falling paper. Physical Review Letter.73, 1372.

STRINGHAM, G.E., SIMONS,D. B., AND GUY, H. P. 1969. The behavior of large particles falling in quiescent liquids. U.S.Geol. Surv. Prof. Pap. 562-c.

VAZUQUEZ, P. AND BALSA, M. 2008. Rendering Falling Leaves on Graphics Hardware, In Journal of Virtual Reality and Broadcasting, Volume 5, no. 2.

WEI, X., ZHAO, Y., FAN, Z., Li, W., SUZANNE, Y., AND KAUFMAN, A. 2003. Blowing in the wind, Proc. of the 2003 ACM SIGGRAPH/ Euro graphics Symposium on Computer Animation (Switzerland), 75-85.

WILLMARTH, W. W., HAWK, N. E. AND HARVEY, R. L. 1964. Steady AND unsteady motions and wakes of freely falling disks. Phys. Fluids 7, 197–208.

ZHONG, H., CHEN, S., AND LEE, C. 2011. Experimental study of freely falling thin disks: Transition from planar zigzag to spiral. Physics of Fluids, Volume 23, Issue 1, 011702-011702.